Supporting Information

Ujwal *et al.* 10.1073/pnas.0809634105

SI Text

Expression, Purification, and Refolding. mVDAC1 construct with 6× histidine tag at the amino terminus was generated by subcloning mVDAC1 encoding gene into pQE9 vector and subsequently transformed into M15 *E. coli* for protein expression. Cells were grown at 37°C for ≈2 h in LB medium to A_{600} = 0.6 and induced for 4 h with 1 mM IPTG. Cells were harvested and resuspended in 50 mM Tris·HCl (pH 8.0), 2 mM EDTA, and 20% sucrose. The resuspended pellet was sonicated and centrifuged (12,000 × *g*, 15 min) to obtain inclusion bodies. The inclusion body pellet was washed with 2 column volumes of wash buffer [20 mM Tris·HCl (pH 8.0), 300 mM NaCl, 2 mM $CaCl_2$], repelleted and solubilized in equilibration buffer [20 mM Tris·HCl (pH 8.0), 300 mM NaCl, 6 M guanidinium hydrochloride (GdnHCl)]. Solubilized inclusion bodies were applied to a Talon metal affinity column, washed with equilibration buffer, and eluted with equilibration buffer containing 150 mM imidazole. Affinity-purified protein was concentrated to 5 mg/ml by using Amicon Ultra-10 concentrators and transferred to a 6- to 8-kDa dialysis bag. Refolding dialysis was carried out in three steps: (*i*) 20 mM Tris·HCl (pH 8.0), 300 mM NaCl, 1 mM DTT, 3M GdnHCl; (*ii*) 20 mM Tris·HCl (pH 8.0), 300 mM NaCl, 1 mM DTT, 2% LDAO; and (*iii*) 20 mM Tris·HCl (pH 8.0), 50 mM NaCl, 1 mM DTT, 2% LDAO. Refolded protein was concentrated by using Amicon Ultra-30 concentrators and ultracentrifuged (355,000 × *g*, 30 min) to remove aggregated protein.

The refolded protein sample was applied to a Superdex 75 column and eluted with SEC buffer [20 mM Tris·HCl (pH 8.0), 150 mM NaCl, 1 mM DTT, 0.1% LDAO] to obtain a homogenous protein population. The eluted peak was washed with 3 volumes of crystal buffer [20 mM Tris·HCl (pH 8.0), 50 mM NaCl, 0.1% LDAO], concentrated by using Amicon Ultra-30 (Millipore) and ultracentrifuged (355,000 × *g*, 30 min). Protein purity and identity were verified by SDS/PAGE, Western blotting, ESI-MS, and tandem mass spectrometry.

Single-Channel Conductance Measurements. diPhPC bilayers were generated across a 0.1-mm hole separating the cis and trans chambers containing 10 mM Tris·HCl (pH 7.4), 1 M KCl, 5 mM $CaCl_2$. One-microliter aliquots of 0.1 μg/mL mVDAC1 were added to the *cis* compartment and stirred. When channel activity appeared, voltages of ±10 to ±60 mV in steps of 10 mV were applied and currents recorded for at least 3 min at each voltage. From the single-channel measurements, the total point histogram at each applied voltage was plotted, and the most frequent conductance was calculated at that voltage. The relative conductance (G_0/G_U) was plotted as a function of the applied voltage, where G_0 is the conductance at 10 mV and G_U is the conductance at voltage U. All experiments were performed at room temperature. The *cis* chamber was the voltage-controlled side, whereas the *trans* chamber was connected to ground. The amplified signal was filtered at 0.5 kHz with an 8-pole Bessel filter viewed with an analog/digital oscilloscope and recorded online. A custom-made software (GpatchM) was used for data collection and analysis.

Crystallization. Purified mVDAC1 protein at 15 mg/mL was mixed with a 35% bicellar solution, giving 12 mg/mL mVDAC1 in 7% bicelles. Crystallization trials, using up to 700 commercially available conditions, were performed by using the hanging drop vapor diffusion method at 20 °C with the Mosquito crystallization robot (TTP Labtech). Initial crystals grew in 0.1 M Tris·HCl (pH 8.5), 15% MPD; 0.1 M Tris·HCl (pH 7.5), 15% ethanol, 0.3 M NaCl; and 0.1 M Tris·HCl (pH 7.5), 9% isopropanol, 0.3 M NaCl. The proteinacious nature of the crystals was confirmed by UV microscopy (Korima). Our best crystals grew in 18–20% MPD, 0.1 M Tris·HCl (pH 8.5) with 10% PEG400 added to the protein drop only (and not in the reservoir). A technical advantage of bicelle mixtures over other lipidic media is the ability to use robotics for crystallization: bicelle mixtures have lower viscosity at low temperature (≈4 °C), but as the temperature increases (to ≈30 °C), the bicelles form a gel that provides a scaffold for type I crystals.

Mercury Labeling. All cysteine constructs were labeled by using a 5-fold molar excess of methyl mercuric acetate (MMA) for 2 h at room temperature before crystallization. Excess MMA was removed by repeated washing with crystal buffer in an Amicon Ultra-30 concentrator. The wild-type sequence, which contains two cysteines at position 127 and 232, did not produce any crystals after MMA labeling. Single-cysteine constructs, mVDAC1-C127A and mVDAC1-C232A, were prepared by using the site-directed mutagenesis kit (Stratagene) by mutating the native cysteines to alanines. The mVDAC1-C232A construct, having the single Cys-127 residue, was successfully labeled and used for structure determination.

Electrostatic Potentials. Electrostatic potentials were calculated by using the nonlinear Poisson–Boltzmann equation, as implemented in APBS version 4.0 (1), at a temperature of 310 K and a salt (NaCl) concentration of 150 mM. Hydrogens were added and optimized at pH 7.4 by using PDB2PQR (2) before performing the APBS calculation.

Identification of Metal Binding Sites. To assess the binding of ions and nucleotides, difference Fourier maps were computed by using the observed structure factor amplitudes for (*i*) Ca^{2+}/mVDAC1 cocrystal, (*ii*) Mg^{2+}-ATP mVDAC1 cocrystal, and (*iii*) EGTA-soaked mVDAC1 crystal and both the observed structure factor amplitudes and the calculated phases of native mVDAC1. Structure factor amplitude differences were Q-weighted to improve the signal-to-noise ratios of the Fourier difference maps (3).

1. Baker NA, *et al.* (2001) Electrostatics of nanosystems: Application to microtubules and the ribosome. *Proc Natl Acad Sci USA* 98:10037–10041.
2. Dolinsky TJ, Nielsen JE, McCammon JA, Baker NA (2004) PDB2PQR: An automated pipeline for the setup of Poisson–Boltzmann electrostatics calculations. *Nucleic Acids Res* 32:W665–W667.
3. Colletier JP, *et al.* (2007) Use of a ''caged'' analogue to study the traffic of choline within acetylcholinesterase by kinetic crystallography. *Acta Crystallogr D* 63:1115–1128.

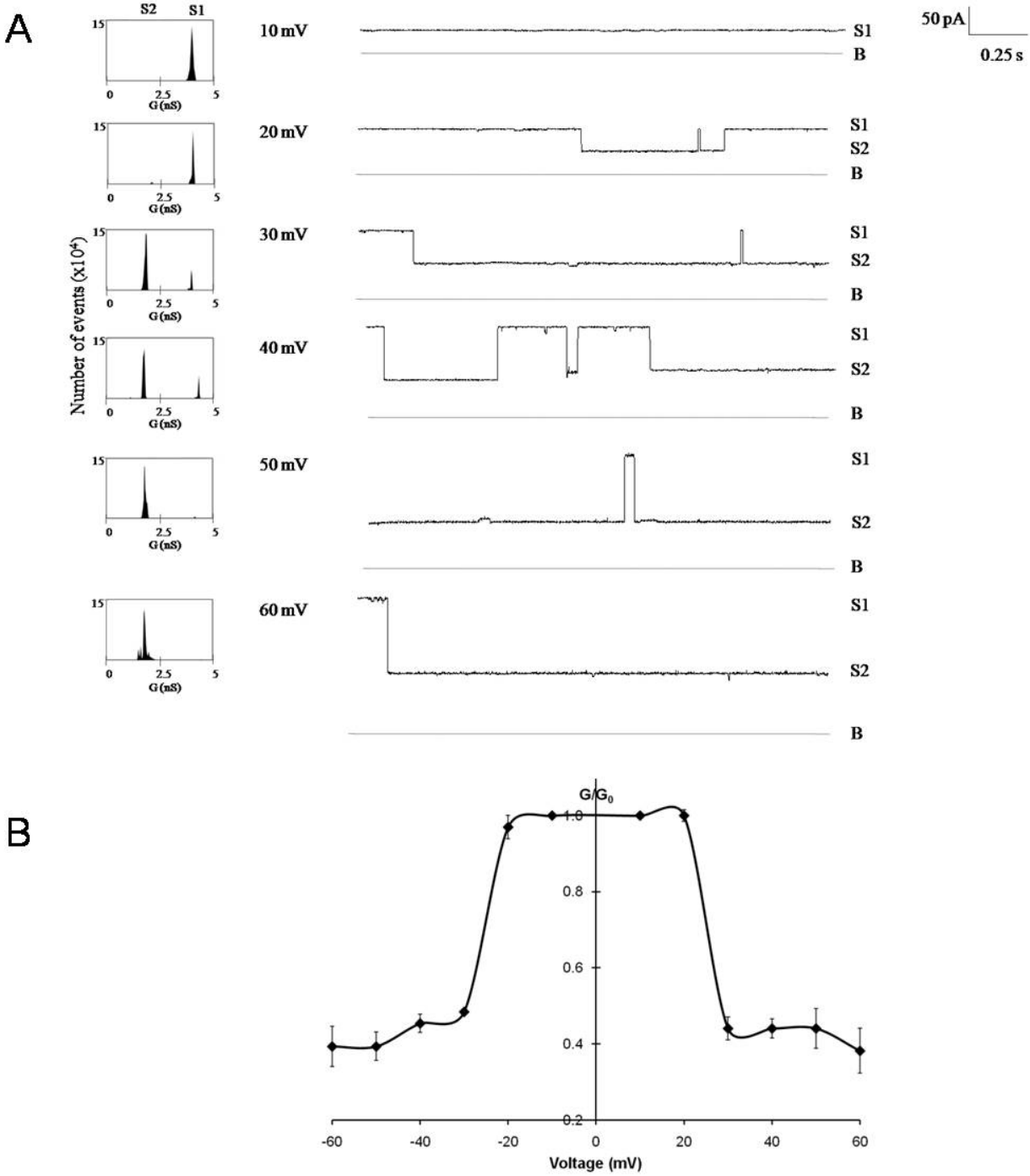

Fig. S1. Electrophysiology experiments on mVDAC1. To ensure that the protein used for crystallization was functional, we examined the electrophysiological properties of purified mVDAC1. (*A*) (*Left*) Total point conductance histograms of mVDAC1 incorporated in black lipid membranes at different applied voltages. The histograms show the 3.7 ± 0.4 nS (S1) and the 1.7 ± 0.2 nS (S2) preferred states during 3-min recordings. (*Right*) Representative current traces at the indicated voltages. At lower voltages ($< \pm 30$ mV), the channel primarily exists in a fully open state (S1) with a dominant conductance of ≈4 nS. As the applied voltage is increased in positive ($> +30$ mV) or negative (< -30 mV) direction, the channel shifts to a predominant subconductance of ≈2 nS (S2). Baseline (B) for each trace is indicated by a dotted line. (*B*) Conductance profile (voltage vs. relative conductance plot) of mVDAC1 shows characteristic voltage-dependent behavior. Mean relative conductances (G/G_0) were calculated as a function of the bilayer voltage; G is the dominant conductance at the applied voltage, and G_0 is the dominant conductance at 10 mV. Bars indicate standard deviations.

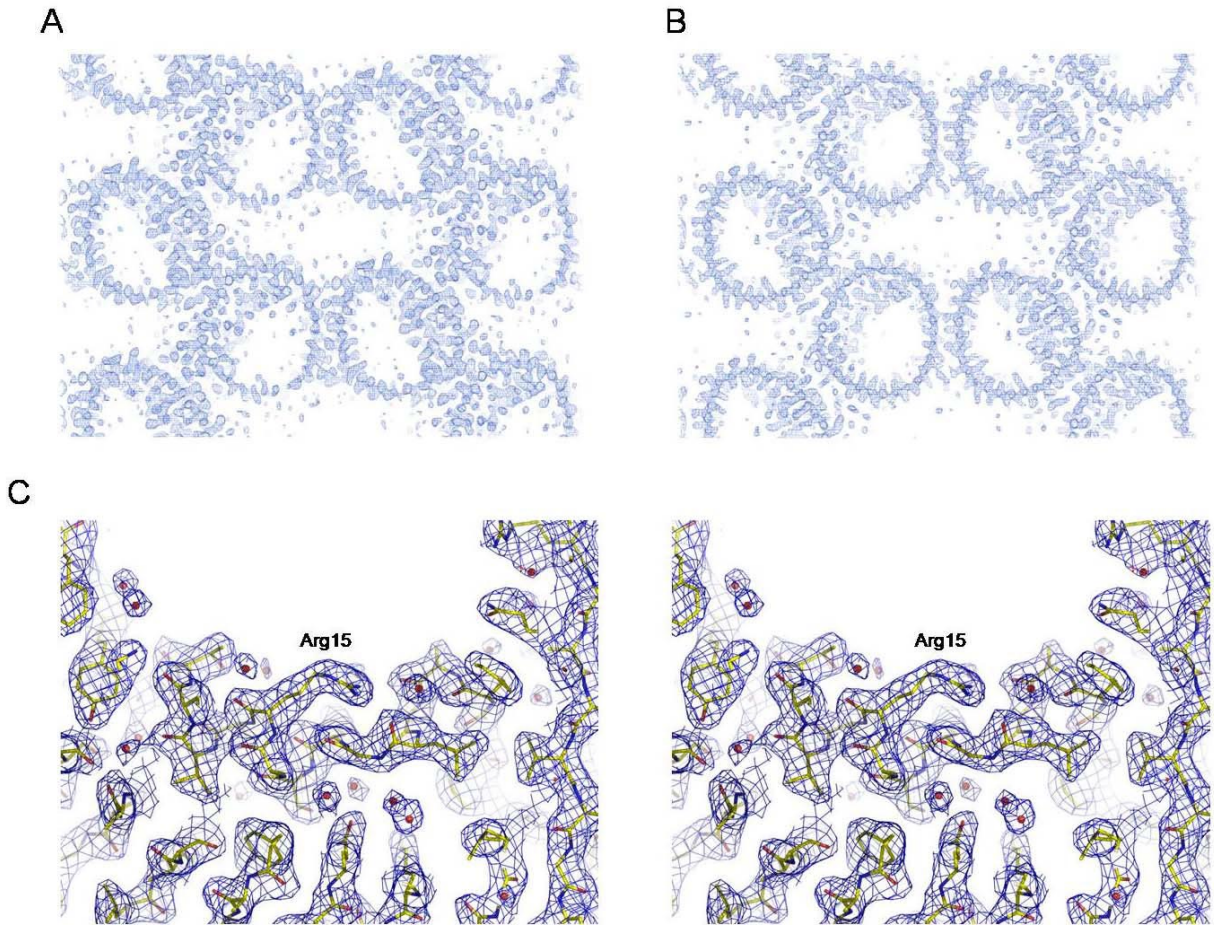

Fig. S2. Electron density maps. (*A*) SIRAS experimental map displayed at 1.2 σ showing the crystal packing. (*B*) Final 2 $F_o - F_c$ map displayed at 1.2 σ showing the crystal packing. (*C*) Stereoview of a close-up of the N-terminal helix. Arg-15 is shown interacting with the main-chain carbonyl oxygen of Ala-8 and Leu-10. The 2 $F_o - F_c$ map displayed at 1.2 σ is superimposed on the model.

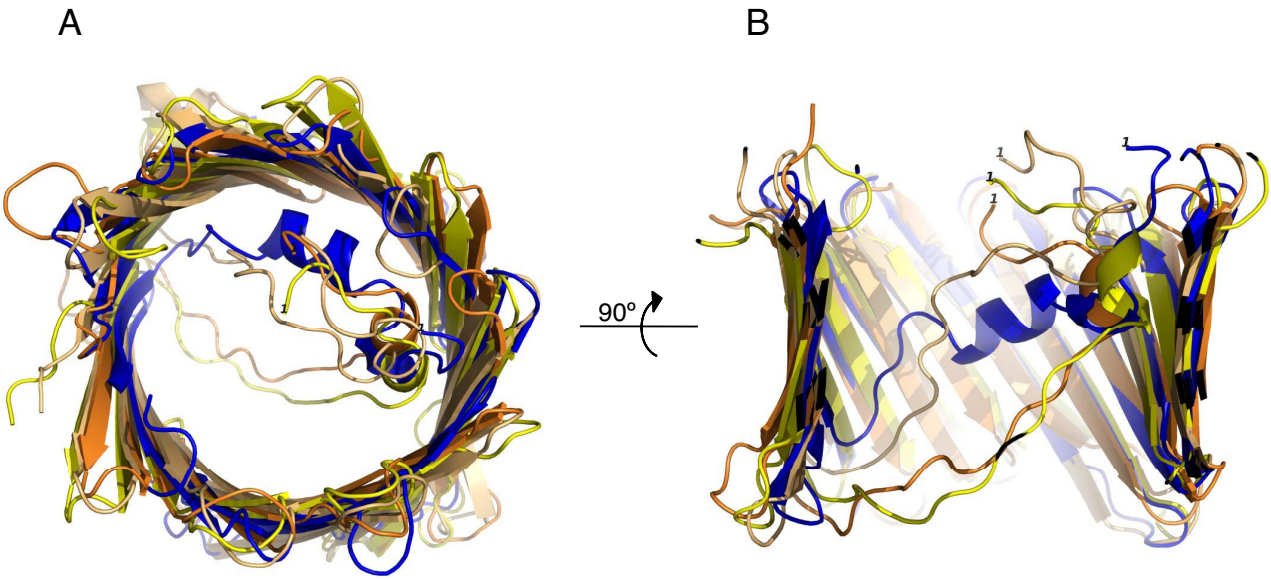

Fig. S3. Overlay of mVDAC1 and hVDAC1. Structural alignment of mVDAC1 (blue) with hVDAC1 (Protein Data Bank ID code 2k4t) NMR models: model 2 (yellow), model 6 (orange), and model 8 (light orange). The average rmsd of the 20 deposited structures of hVDAC1 is 4.79 Å, whereas that between those structures and mVDAC1 ranges from 1.72 to 4.68 Å. Models 2, 6, and 8 are those with the lowest rmsd values (<2 Å). The N terminus of each model is numbered. (*A*) Viewed perpendicular to the plane of the membrane. (*B*) Cross-section view parallel to the plane of the membrane.

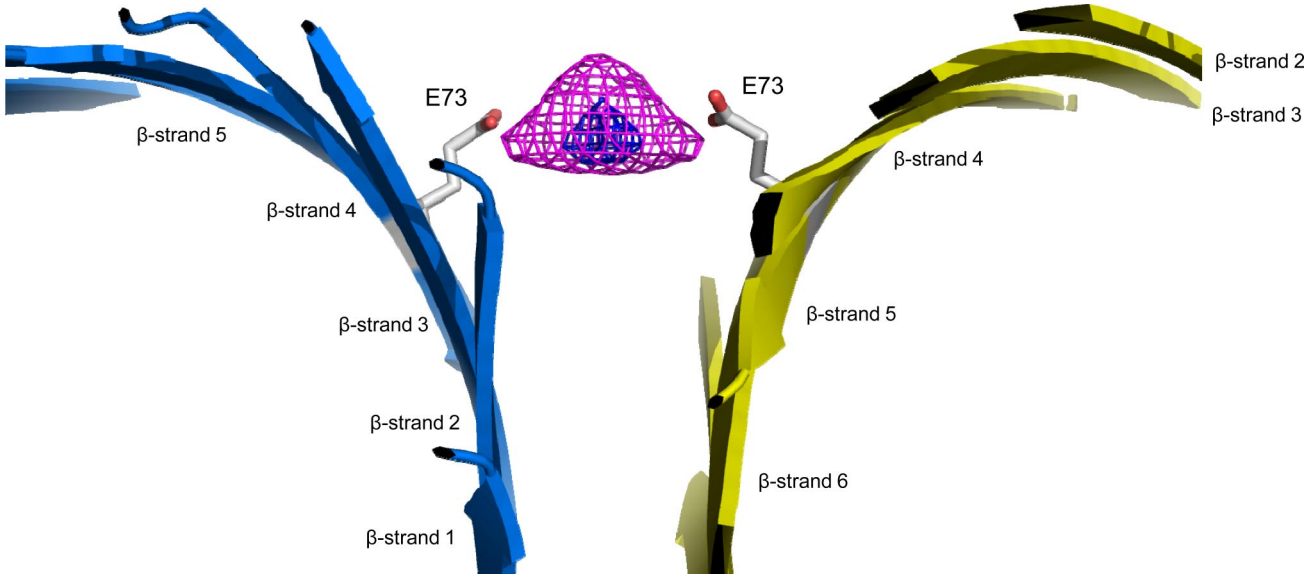

Fig. S4. $F_o - F_c$ maps showing localization of Ca^{2+} and Mg^{2+} along the mVDAC1 dimer interface. The difference Fourier maps ($F_o - F_c$) were computed by using the observed structure factor amplitudes for Ca^{2+}/mVDAC1 and Mg^{2+}-ATP/mVDAC1 cocrystals and both the observed structure factor amplitudes and the calculated phases of mVDAC1 in the absence of these compounds. Structure factor amplitude differences were Q-weighted to improve the signal-to-noise ratios of the Fourier difference maps. Maps for Ca^{2+} and Mg^{2+} are colored blue and pink, respectively. Both maps are contoured at 4.5 σ.

Table S1. Statistics for crystallographic data collection and refinement

	Native	Hg derivative
Wavelength, Å	1.0	0.9792
Space group	C2	C2
Unit Cell abc, Å	100.23, 58.39, 66.58	98.95, 57.97, 66.81
$\alpha\beta\gamma$, °	90, 99.25, 90	90, 97.94, 90
Resolution, Å	20–2.3 (2.3–2.4)	50–2.9 (3.0–2.9)
R_{merge}, %	2.9 (47.1)	9.6 (29.1)
Completeness, %	97.5 (98.7)	99.7 (98.9)
Redundancy	3.2 (3.2)	5.3 (3.4)
I/σ	24.1 (2.6)	25.7 (3.4)
No. of unique reflections	16,629 (2,010)	8,364 (815)
R_{work}/R_{free}	27.7/24.2	
rmsd bonds, Å	0.014	
Angles, °	1.768	
SIRAS phasing statistics		
R_{Cullis} (acentric/centric)	0.75/0.68	
Phasing power (acentric/centric)	1.96/1.61	
Figure of merit	0.42	
Figure of merit (after density modification)	0.67	

The values in parentheses refer to the highest-resolution shell. $R_{merge} = \Sigma_i|I_i - <I>|/\Sigma_i|I_i|$, where I_i is the intensity of the i reflection. $R_{work} = \Sigma||F_o| - |F_c||/\Sigma|F_o|$. $R_{Cullis} = \Sigma||F_{PH} \pm F_P| - |F_{PH\ (calc)}||/\ \Sigma|F_{PH} - F_P|$. *Phasing power* $= |F_{H(calc)}|/\Sigma||\ F_{PH} \pm F_P| - |F_{PH\ (calc)}||$.